Appl. Phys. B 85, 199–206 (2006)
DOI: 10.1007/s00340-006-2311-1

Applied Physics B
Lasers and Optics

S.E. BISSON[1,✉]
T.J. KULP[1]
O. LEVI[2]
J.S. HARRIS[2]
M.M. FEJER[2]

Long-wave IR chemical sensing based on difference frequency generation in orientation-patterned GaAs

[1] Sandia National Laboratories, Livermore, CA 94551-0969, USA
[2] E.L. Ginzton Laboratory, Stanford University, Stanford, CA 94305, USA

Received: 6 April 2006/Revised version: 9 May 2006
Published online: 23 June 2006 •

ABSTRACT The combination of continuous-wave difference frequency generation based on quasi-phase-matched (QPM) gallium arsenide with cavity ring-down spectroscopy is explored for use in spectroscopic and chemical sensing applications. The advent of QPM materials based on orientation-patterned GaAs (OP-GaAs) offers a significant advantage over traditional ferroelectric QPM materials of extended wavelength coverage into the spectroscopically important 8–12 μm region. In this work, the outputs from two tunable, external cavity diode lasers covering the 1.3 μm and 1.5 μm telecom bands were amplified then mixed in an orientation-patterned GaAs crystal, producing several microwatts of tunable radiation in the 7–9 μm region. We also evaluate the use of a low-power DFG source for use in cavity ring-down spectroscopy.

PACS 82.80.Gk; 42.62.Fi; 42.70.Hj; 42.65.Ky

1 Introduction

The use of quasi-phase-matched (QPM) materials in spectroscopy and chemical sensing is now well established in the mid-infrared (IR) spectral region (3–5 μm) [1–7]. The ability to tune continuously over broad spectral ranges and to operate at high conversion efficiency in pulsed, continuous-wave and ultra-fast regimes makes these materials highly desirable for many applications. Furthermore, the materials are typically ferroelectric, allowing ease of manufacture and low cost. Their use, however, has been restricted to the mid-IR, typically at wavelengths shorter than 4.5 μm, due to intrinsic absorption. The long-wave IR, defined herein as the 8–12 μm atmospheric window, offers many potential advantages for chemical sensing in that more functional groups absorb in this region, atmospheric transmission is generally good and depending on the particular functional groups, absorption strengths can be stronger than in the mid-IR. Until recently, the extension of QPM to the long-wave region has been elusive due to the lack of QPM materials that can operate in this region. During the last several years however, researchers at Stanford University have succeeded in developing analogous long-wave QPM materials based on orientation patterned GaAs (OP-GaAs) [8]. As GaAs is not amenable to electric field poling, it must be grown with the optical axis periodically reversed. Fabrication of orientation patterned GaAs employs both thin film molecular beam epitaxy (MBE) and thick film hydride vapor phase epitaxy (HVPE) growth techniques. The use of MBE growth methods and standard semiconductor materials offers the possibility of highly integrated devices, employing both waveguide structures and active sources. The combination of a broad transparency range (∼ 1–17 μm) and a high nonlinear coefficient (90 pm/V) make OP-GaAs desirable for long-wave infrared generation where high efficiency is required. These attributes greatly relax constraints on the pump sources, allowing the use of mature, commercial sources such as those available in the telecommunication bands. OP-GaAs enables for the first time, broadly tunable, continuous wave, long-wave IR sources. In this work, we evaluate an OP-GaAs difference frequency generation source for use in long-wave IR chemical sensing and demonstrate initial application to cavity ring-down spectroscopy. The broad tunability of this source, coupled with the sensitivity of cavity ring-down spectroscopy (CRDS), will enable both highly sensitive detection and identification of a broad range of species.

2 Experimental

2.1 *Source requirements*

The combined requirements of highly sensitive detection and the need to detect a broad range of species – both broad and narrow line absorbers – places stringent requirements on the IR source. The choice of cavity ring down spectroscopy (CRDS) offers high sensitivity and selectivity to molecules with both broad and narrow spectral features and requires little power (μW), which relaxes source power requirements. These are important attributes as other methods such as frequency modulation spectroscopy, while extremely sensitive to species with narrow line features are insensitive to broadly absorbing features. Thus, an entire class of species (i.e., large molecular weight) could be excluded from measurement. CRDS is sensitive to loss only and is independent of the spectral characteristics. For maximum sensitivity, single frequency, continuous-wave (cw) operation is preferred for eliminating mode beating and ensuring a single exponential ring-down decay. However, this introduces the complication of overlapping the input frequency with a resonance of the ring-down cell. Continuous-wave operation is also amenable to high data acquisition rates, allowing rapid signal averaging. As the ring-down cell resonances can be very narrow, i.e.,

✉ E-mail: sebisso@sandia.gov

10–100 KHz, a narrow linewidth source is also required for good throughput. Also, some means must be employed to ensure overlap of the narrow cavity ring-down resonance with the IR source i.e., dithering of the input frequency or ring-down cell mirror. The final requirement is broad tunability (several hundred wavenumbers) with either continuous tuning or fine steps (< 100 MHz). While many sources operate in this range, they do not have the required spectral coverage and the continuous tuning range is usually much less than the spectral coverage.

Devices based on direct infrared generation, such as quantum cascade lasers (QCLs) [9], have relatively high power (10–100 mW) and are available throughout a broad spectral range, but are designed for a specific wavelength range and to date have limited continuous tuning capability. More versatile external cavity QCLs have been demonstrated with broad tuning (35 cm^{-1}) although continuous mode-hop free tuning was performed in 1–2 cm^{-1} ranges [10]. Other sources, such as CO_2 lasers are limited to discrete frequencies. In contrast, indirect methods of infrared generation, i.e., those employing nonlinear frequency conversion, can have extremely broad tunability and high power. Optical parametric oscillators are commonly used for nonlinear frequency conversion and can have broad tunabiltiy with high power but the tuning must be engineered into the system. For spectroscopic grade sources such as required here, this is a challenging task. In the case of difference frequency generation (DFG), highly engineered tunable pump sources can be used, thus eliminating the requirement to develop complicated tuning systems. However, DFG systems based on traditional birefringently tuned crystals are inefficient, requiring larger pump sources and mechanical tuning of the crystal. In contrast, QPM materials can exploit the highest nonlinear coefficient and can operate throughout the entire transparency range of the crystal. For spectroscopic and chemical sensing applications where broad tuning is required, difference frequency generation based on QPM materials offer the prospect of compact, practical infrared sources [11, 12]. Tittel et al. have published several reviews of IR sources and their application to spectroscopy [13, 14].

For these reasons, we have selected cw, difference frequency generation in orientation patterned GaAs (OP-GaAs). This approach offers broad tuning throughout the long-wave infrared, combined with the simplicity of using highly engineered, tunable pump sources [15, 16]. Although the output power is typically low for cw difference frequency generation, cavity ring-down spectroscopy can be performed at the μW level. This work serves to demonstrate the application of OP-GaAs to spectroscopy and chemical sensing problems. While the output power may be somewhat low for cw cavity ring-down spectroscopy, future implementations of OP-GaAs may offer higher power enabling more precise spectroscopic measurements.

2.2 DFG *system*

A schematic of the combined DFG/cavity ring-down system is shown in Fig. 1. In this approach, the outputs from two tunable sources operating in the telecom bands, one in the 1550 nm "C" band and another in 1300 nm "O" band were mixed in OP-GaAs to generate tunable long-wave infrared radiation. Extensive use of telecom technology was used to simplify tuning, beam delivery and ensure high beam quality.

The C band source was based on a 2 W, cw IPG Photonics polarization maintaining (PM) erbium doped fiber amplifier, model EAD-2 (IPG Photonics Corp. Oxford, MA 01540, USA). The seed source was a fiber-coupled, 10 mW, frequency agile, single mode, external cavity diode laser (ECDL) from New Focus, model TLB 6500 C which was tunable without mode-hops from 1520–1580 nm (New Focus, 2584 Junction Ave., San Jose, CA 95134, USA). However, the gain bandwidth of the erbium doped fiber amplifier restricted tuning from 1530–1567 nm. A fiber-coupled, acousto-optic modulator was placed between the seed laser and erbium fiber amplifier for switching of the ring-down signal. This introduced the complication of a temporarily unseeded erbium amplifier, but was the most efficient method compared to direct switching of the erbium fiber amplifier output. To avoid a potentially damaging unseeded condition, a second, fixed wavelength (1567 nm) distributed feedback diode laser was switched into the erbium fiber amplifier to pull the gain down to saturated levels. This ''off'' wavelength was set at the extreme edge of the erbium amplifier gain bandwidth to avoid phase matching in the OP-GaAs crystal. For the ring-down decay times observed here (1–4 μS), an off time of approximately 10 μS–20 μS was required to optimally observe the decay. The seeded output power of the erbium amplifier was manually varied between 1–1.75 W, with nearly constant power over the tuning range.

The O band source wad based on a 20 m length NEL praseodymium-doped fiber amplifier module, model FFM-I-Pr-1000-A-20-F (NEL America, Inc. Saddle Brook, NJ 07663, USA) which was also seeded by a frequency agile New Focus ECDL, model TLB 6500 O, that tuned from 1260–1340 nm. Since praseodymium-doped fiber amplifiers are based on fluoride fiber technology [17, 18] and are not available in PM formats, a double pass configuration with a Faraday mirror [19] was used (Micro-Optics, Inc, Hackettstown, NJ 07840-4227). This yielded linear polarized light over the entire praseodymium gain bandwidth from 1280–1320 nm. In principle, the cubic crystal symmetry of

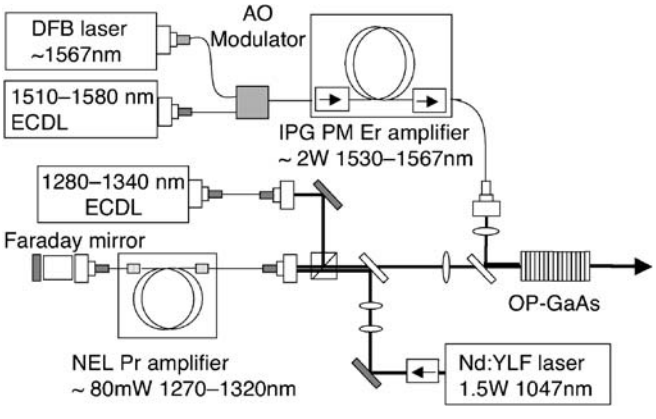

FIGURE 1 Simplified schematic of DFG system. The praseodymium amplifier is a double-pass configuration with the input and output on the same end

GaAs allows unpolarized light to be used; however, the crystal used in this work appeared to have some residual birefringence. To explore this, we demonstrated difference frequency generation with both pump waves polarized parallel and with orthogonal polarizations. While the peak phase matching wavelengths were expected to be the same for either polarization configuration, a shift of 0.6 cm^{-1} was observed, which is approximately one half of the phase matching bandwidth at these pump wavelengths. Thus, it may be difficult to use an unpolarized pump wave at these wavelengths. However, this may be less of an issue at longer pump wavelengths where the phase matching bandwidths are larger. The double-pass architecture of the praseodymium amplifier also made the system highly susceptible to relaxation oscillations, which could drive parasitic nonlinear phenomenon in the fiber, possibly creating transient emissions at other wavelengths. This was mitigated to some extent by reducing feedback external to the amplifier, primarily through the use of angle polished, FC/APC fiber connectors. A 1.5 W Nd:YLF laser (Crystal Laser IRCL-1.5w-1047) was used to pump the praseodymium fiber amplifier ($\sim$ 800 mW of injected power), which yielded a double pass output power of up to 80 mW for 5 mW of injected seed power.

The outputs of both fiber amplifiers were collimated with OFR 11 mm focal length fiber ports, model PAF-X-11 (OFR Inc, Caldwell, NJ, 07006 USA), and were combined with a dichroic beam combiner. A Spiricon (Spiricon Inc, Logan, UT 84341 USA) near-IR pyrocamera was used to verify the collimation of the beams and to adjust the fiber ports for minimum astigmatism. Improperly aligned ports could introduce astigmatism due to their use of short focal length, aspheric lenses. This was important for optimizing the DFG conversion efficiency and for efficient mode matching into the cavity ring-down cell.

Once the beams were collimated and combined, a 20 cm focal length lens was used to focus the beams into the OP-GaAs crystal. The confocal beam parameters were adjusted to be one half of the crystal length ($l = 18$ mm). This condition was chosen over the optimized Boyd and Kleinman [20] condition partly because the useable crystal thickness restricted the beam waist at the crystal edges. Furthermore, analytical solutions require equal confocal beam parameters and that the difference wave is resonated.

The OP-GaAs crystal used in this work was 19 mm long, $\sim$ 500 μm thick and was patterned with a single 26.3 μm period. This period provided phase matching in the 7–9 μm spectral region with 1300 and 1550 nm tunable pump sources. While broad tuning could be achieved through pump tuning alone, this range can be extended by temperature tuning of the GaAs crystal. For this reason, the crystal was mounted in an oven that allowed temperature tuning from room temperature ($\sim$ 25 °C) to approximately 100 °C. Due to growth fidelity issues, there were many irregularities observed in the crystal, both in the growth direction and transverse directions. This required precise positioning of the crystal in the pump beams to optimize the output power. A near infrared pyrocamera was also used to observe any pump beam clipping or beam distortions induced by crystal defects. The crystal facets were uncoated and thus exhibited high Fresnel reflection losses for all wavelengths. The generated difference frequency wave was observed with a 256×256 liquid nitrogen cooled mercury cadmium telluride array detector (Santa Barbara Focalplane, Goleta CA, 93117) with a cold filter centered near 8.0 μm to reduce out of band thermal radiation. Figure 2 illustrates a DFG beam image acquired by focusing into the camera and with only a few microwatts of power. The slight asymmetry appears to be an external etalon effect as verified by tuning of the DFG wavelength. The low DFG power combined with the thermal background made detailed quantification of the beam difficult.

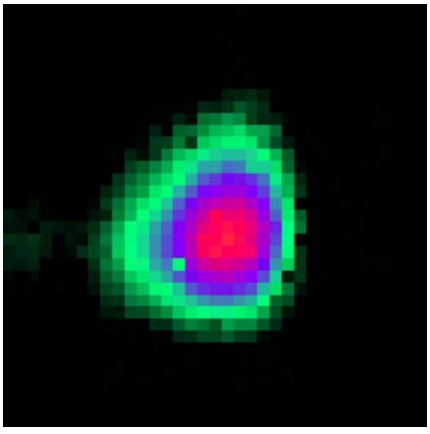

FIGURE 2 Infrared image of the generated 8.0 μm beam. The slight asymmetry was due to etaloning in the camera cold filter. This image was acquired with a liquid nitrogen cooled 256×256 MCT array camera with a narrowband cold filter

2.3 *Tuning*

The output wavelength of the DFG source was scanned by simultaneously tuning both of the seed sources. The 1300 nm "O" band source was typically tuned in fixed steps of 0.001 nm while the 1550 "C" band source was tuned in the same direction but with varying step sizes to maintain phase matching. An empirically derived quadratic polynomial was used to determine the appropriate C-band wavelength. While the quadratic term was necessary to maintain phase matching, it was small compared to the linear term, which resulted in reasonably linear tuning for the output. The above step sizes for the pump waves corresponds approximately to 0.0035 cm^{-1} or 2.3×10^{-5} nm in the long-wave infrared. Depending on the pump power used at 1550 nm (1–2 W) a small positive offset (usually 0.02–0.04 nm) was added to the empirically derived wavelength to account for pump heating of the OP-GaAs crystal, which moved the phase matching peak slightly. For a fixed crystal period and temperature, the output frequency could be tuned over approximately 50 cm^{-1} or 350 nm; a range that was limited by the tuning range of the pump sources and dispersion in the crystal. Dispersion is an issue when the pump wavelengths are near the crystal bandgap as the pump sources must be tuned simultaneously over a wide range to achieve appreciable tuning at the difference frequency. High linear dispersion translates into narrow phase-matching bandwidths (Fig. 3) and requires more stringent temperature and frequency control.

The spectral region of operation can be moved by temperature tuning of the GaAs crystal, thus extending the effective

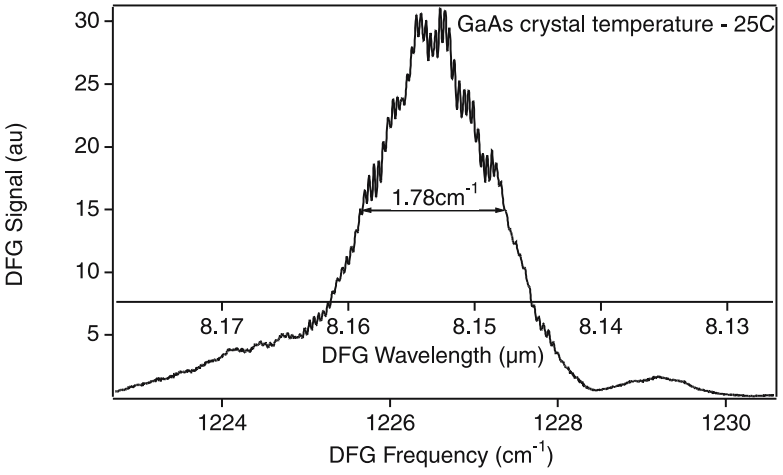

FIGURE 3 DFG scan with one of the pump wavelengths held fixed. The narrow phase matching bandwidth required that both pump wavelengths be tuned to achieve broad scans. The deviation from sinc^2 behavior was seen at all wavelengths and is not currently understood. The high frequency oscillations in the phase matching peak are due to etalon effects in the GaAs crystal

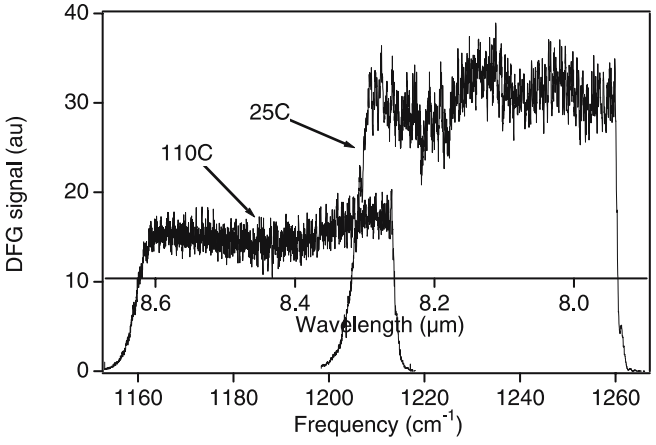

FIGURE 4 Single frequency, high resolution, 50 cm^{-1} DFG scans obtained with a single 26.8 μm period OP-GaAs crystal. The spectral region was set by the temperature of the GaAs crystal whereas the width of the scan was limited by the tuning range of the diode lasers. The appearance of high frequency noise results from etalon effects in the GaAs crystal

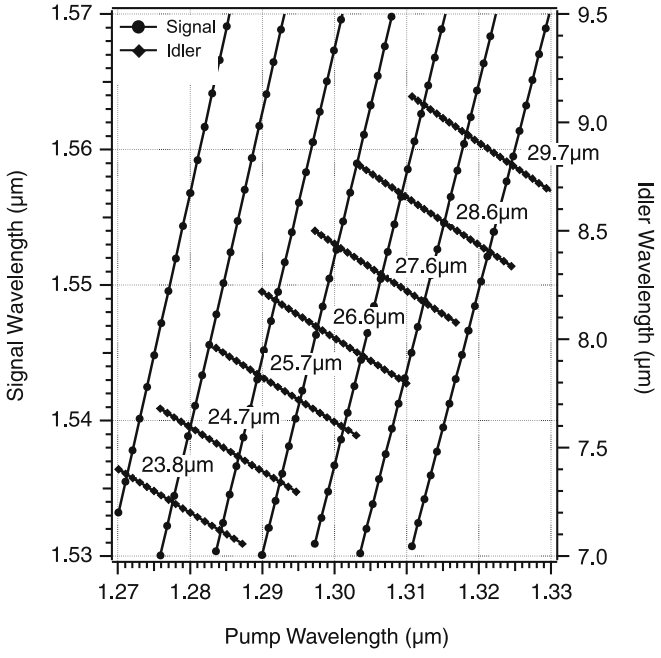

FIGURE 5 Tuning ranges achievable with a multi-grating crystal and tunable telecom sources in the 1550 nm and 1300 nm bands

tuning range. Since the crystal used in this work had a single period (26.3 μm), this was the only method of determining the spectral region of operation. The measured single-period tuning range is shown in Fig. 4 for crystal temperatures between 25 °C and 110 °C. Figure 5 illustrates theoretical tuning ranges achievable with a multi-grating crystal at 30 °C for the pump sources used here. These tuning curves were obtained using the dispersion data of Pikhtin and Yaskov [21]. Because both pump wavelengths were tuned in the same direction but at different rates, very fine-tuning in the long-wave infrared could also be achieved. This is illustrated in Fig. 6 which shows a 10 cm^{-1} scan monitored by a solid 3 mm thick, uncoated germanium etalon at near normal incidence. High finesse etalons were similarly used to monitor the pump sources and verify single frequency tuning. While the linewidths of the pump sources were on the order of several hundred kHz, the ultimate resolution of the system was set by the mode spacing of the cavity ring-down cell (∼ 283 MHz). Furthermore, the frequency increments in the acquired spectrum were somewhat random due to a 400 MHz dither imposed on the DFG signal by the pump sources. This frequency dithering was necessary to ensure overlap of the DFG frequency with a fixed frequency mode of the cavity ring-down cell. For these reasons, cavity ring-down measurements were performed at atmospheric pressure, for which absorption linewidths were large compared to the cavity ring-down mode spacing. This produced a near continuum of measurements. For operation at low pressures (few Torr) where the linewidths are narrow and Doppler broadening is dominant, the cavity ring-down cell resonance must be dithered at least one free spectral range combined with a smaller modulation on one of the pump sources to cover the absorption line. In this work, we have chosen to dither the input frequency rather than the cavity ring-down cell modes solely for ease of implementation. This is discussed further in Sect. 2.4.

2.4 *Cavity ring-down*

The cavity ring-down cell was composed of two highly reflecting ZnSe mirrors (∼ 99.98% at 7.5 μm) spaced approximately 53 cm apart in a stainless steel cell (Fig. 7). The central portion of the cell was a stainless tube with a 0.63 cm

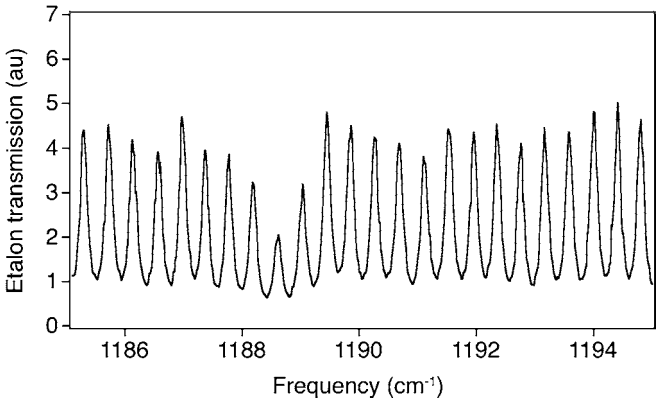

FIGURE 6 High resolution, long-range ($> 10\,\mathrm{cm}^{-1}$) scan monitored by a 3 mm germanium etalon at normal incidence. The source of the low frequency intensity variations have not yet been identified

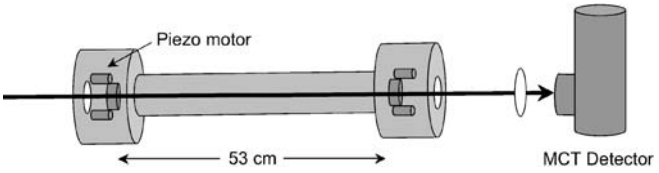

FIGURE 7 Configuration of the cavity ring-down cell and MCT detector. The ring-down mirrors were mounted inside the cell to avoid any potential pressure differential or stress that could cause misalignment. Tunable piezo-electric motors were used to adjust the mirror alignment once the cell was sealed

wall thickness and an outside diameter of 3.8 cm. This produced both mechanical and thermal stability. The ends of the cell contained cylindrical housings ($\sim$ 10 cm diameter by 7.6 cm long) for the ring-down mirrors and piezo-electrically aligned mirror mounts. This avoided having any pressure differential across the ring-down mirrors that could cause alignment issues. The drawback of this approach is that the cell volume was large, resulting in long gas exchange times, which favored static operation. The cell could operate at any pressure from a vacuum for background measurements to several atmospheres but was restricted to ambient temperature. The mirror radii of curvature were 2 m, yielding a mode spot size ($2\omega_0 = 264\,\mu\mathrm{m}$) at $\lambda = 8.0\,\mu\mathrm{m}$. The use of longer, 6 m radii of curvature mirrors, was also explored, but these were of higher reflectivity, which reduced the optical throughput to unacceptably low levels. In either case, the spacing between the ring-down mirrors was fixed so the actual spectrum consisted of discrete measurements spaced a free spectral range of the cavity ($\sim$ 283 MHz). As a result, operation was restricted to atmospheric pressure, where spectral lines are several GHz wide. Piezo electric tuning of the ring-down cell resonances has been demonstrated with this cell, but the large mirror mass, coupled with the use of a single piezo-electric element resulted in some mirror misalignment with corresponding noise in the ring-down decay times. Instead, overlap of the input frequency with the ring-down cell resonance was achieved by dithering both of the diode seed lasers at a rate of approximately 100 Hz in opposite directions over a 200 MHz range. This approach is similar to that used by Schulz et al. [22]. By dithering the diode seed laser frequencies in opposite directions, the total dither range could be increased while reducing the chance for a mode hop. While dithering of the diode seed lasers guarantees overlap with a cavity mode, it restricts the data acquisition rate to the 100 Hz level, owing to the cavity "ring-up" time. This repetition rate restriction can be partially overcome by either locking to a cavity mode or by using a search algorithm with a small dither once the resonance has been found.

Once the source was resonant with a cavity mode, the input light was switched off, in this case by switching the 1550 nm seed source with an AO modulator. The ring-down signal was then detected with a liquid-nitrogen-cooled mercury cadmium telluride (MCT) detector. Because the throughput of the ring-down cell was low ($< 5\%$ and decreasing with shorter wavelengths) and the input power was on the order of 2 μW, the peak ring-down signals could easily be a 100 nW or less. Thus, it was critical to reduce background noise sources, i.e., thermal and electronic. The detector used in this work was a Kolmar MCT model KMPV9-0.5-J1 internally amplified, 0.5 mm detector element with a peak responsivity at 8.8 μm (Kolmar Technologies, Inc, Newburyport, MA 01950). Thermal background incident on the detector was partly mitigated by reducing the detector field-of-view from the standard 60° to 30° (full angle) and adding a germanium cold filter to block radiation shorter than 6.5 μm. Radiation longer than 9.0 μm was eliminated by optimizing the detector material to cutoff beyond 9.0 μm. Signals were further amplified with a custom low bandwidth (< 5 MHz), low noise amplifier and acquired with a 12 bit, 500 MSample/S transient digitizer. Sample rates were typically set around 50 MSample/S.

Electronic noise was reduced by using a transimpedance amplifier mounted just outside the detector dewar that was matched to the detector with a bandwidth of 5 MHz. These modifications increased the d^* from 5.9×10^{10} Jones to 1.7×10^{11} Jones (measured at 10 kHz), resulting in a theoretical noise equivalent power of 700 pW. For a transimpedance gain of 2.26×10^5 V/W, this corresponded to a noise equivalent voltage of 158 μV, however, the actual noise levels were on the order of several mV, probably due to external noise sources and the non-ideal frequency response of the detector/transimpedance amplifier combination. When the output of the detector was observed on a spectrum analyzer, two noise peaks were observed in the MHz range. The quoted d^* was based on a low frequency measurement and so simple NEP calculations were not valid. For this work, the full 5 MHz bandwidth of the detector was not required, so an in-line Mini-Circuits 1.9 MHz bandpass filter was installed (MiniCircuits, Brooklyn, NY 11235 USA). The use of narrower bandwidths resulted in a distortion of the ring-down signal. Thus, the detector noise floor was fixed at approximately 2 mV with amplification. While the single shot, peak signal to noise ratio was in general good ($\sim$ 10–50 : 1), the signal amplitude was still too low for accurate single shot ring-down measurements so 100 averages or more were typically acquired per wavelength.

To ensure the highest signal to noise ratio, it was essential to reduce optical inefficiencies in the system, such as the ring-down cell throughput, Fresnel losses of the high index GaAs crystal ($n \sim 3.5$) and optical switching losses. The latter were reduced by optimal placement of the switch, which was positioned between the 1550 nm diode seed laser and

erbium amplifier. Electro–optic switching offered both high efficiency and speed, but produced intolerable rf interference in the MCT detector. Acousto–optic switching offered reasonable speed (~ 50 ns) without rf interference, but efficiencies were typically around 50%. For this reason, the switch was installed between the 1550 nm diode seed laser and erbium amplifier. Since the erbium amplifier was operated in a saturated condition, the output power was relatively insensitive to the seed power. However, when the seed was switched off for more than about 10 μs, the erbium amplifier gain could build up to high levels, possibly damaging the amplifier. To suppress this gain build-up, an off-wavelength diode seed laser was switched into the erbium amplifier during the ring-down decay.

Absorption spectra were acquired by averaging a fixed number (typically around 50–100) of ring-down measurements per wavelength, then computing the average ring down loss per pass (combined cavity and absorption losses). The DFG source was then stepped to the next wavelength and the process repeated until the desired spectral range was covered. Since the cavity ring-down mirrors were fixed, the minimum step size was the cavity ring down cell free spectral range or approximately 283 MHz.

3 Results and discussion

Figure 8 shows an example of a high-resolution ($0.0035\,\mathrm{cm}^{-1}$ per point), background subtracted, CRDS scan of N_2O over a $20\,\mathrm{cm}^{-1}$ range. For this scan, the cell was filled with a mixture of 15 ppm N_2O in balance nitrogen at sea level atmospheric pressure. Some residual water vapor is also evident. Baseline ring-down cell losses were determined by purging the cell with dry nitrogen and recording the ring-down decay over the same spectral range. This was used to subtract out the wavelength-dependent cavity loss (mirror reflectivity) from the gas absorption. The ring-down cell throughput and decay rate also exhibited a strong dependence with wavelength (Fig. 9). We have also observed that a significant contribution to the ring-down noise (given in loss per pass) is related to the stepping of the wavelength. The cause of this is unknown, but ring-down mode variability could be a contributor. Calculations based on SNLO [23] indicate that a phase mismatch of ± 0.5 /mm can cause significant mode variability as observed in the far-field; however, this can be easily controlled through active temperature and frequency control.

Anderson [24] and Sampas [25] have shown that off-axis translations and off-axis alignment of a coherent optical beam can each excite characteristic modes in an optical cavity. Thus, in principle, it may be possible to diagnose higher order modes based on imaging of the transmitted beam or on their frequency spacing. However, due to the low transmitted power through the ring-down cell (< 100 nW) direct imaging of the transmitted ring-down beam was not possible. When the wavelength was held fixed, the ring-down noise was significantly less, on the order of $2\text{–}5 \times 10^{-6}$ per pass loss as compared to the $2\text{–}10 \times 10^{-5}$ for the case where the lasers were tuned. Each point in the ring-down decay is an average of 50–100 ring-down measurements fitted in real-time to an exponential. Fit parameters such as the starting and ending points could be adjusted in manually in real time to account for varying ring-down decay rates or noise. Typical acquisition sampling rates were 50 MSamples/S, which is oversampled given the combined detector/amplifier bandwidth (1.9 MHz). Given that the DFG power was in the μW range and that the cell throughput was low ($\sim 1\%\text{–}5\%$) the ring-down decay could only be fit over two lifetimes. This, combined with a somewhat noisy signal, prevented determination of accurate ring-down decay rates and restricted measurements to the ppm concentration range.

While this sensitivity was somewhat low, it serves as a baseline to predict performance of higher power systems. In particular, we have developed a semi-empirical model that incorporates detector noise, ring-down mirror reflectivity, cell throughput, signal averaging, etc. to evaluate ring-down performance as a function of operational parameters such as power, wavelength and noise. Specifically, using a least squares fit to an exponential ring-down decay, an analytic expression for the ring-down decay time was derived. The dependence of the calculated ring-down decay time was then evaluated as a function of stochastic noise. The variability in ring-down decay was then related to the

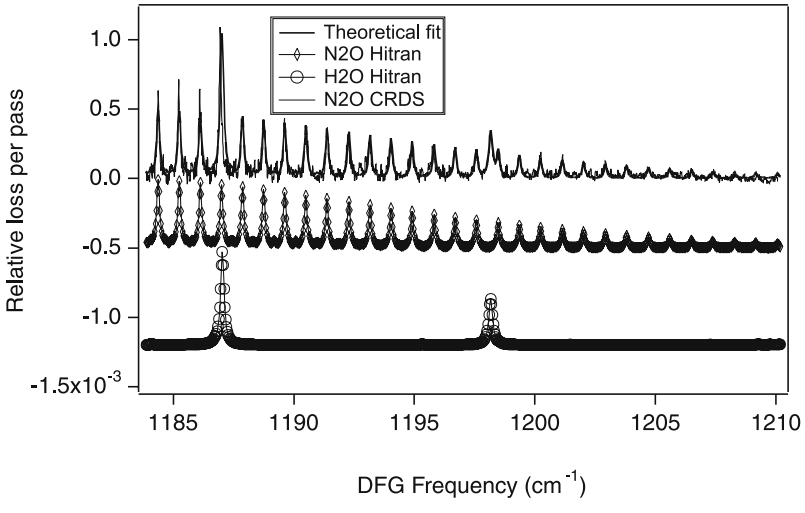

FIGURE 8 Measured ring-down spectrum of 15 ppm N_2O in balance nitrogen at atmospheric pressure. Theoretical HITRAN spectra of N_2O and water vapor are shown for comparison. Some residual water vapor is evident. These measurements were acquired with an OP-GaAs crystal temperature of 70 °C

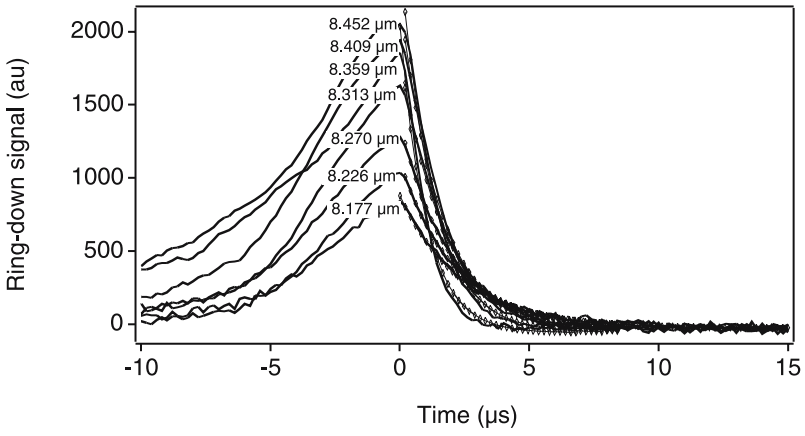

FIGURE 9 Actual ring-down decays for various wavelengths in the 8.0 μm region. Note the reduction in the peak ring-down decay with decreasing wavelength. This is a result of reduced ring-down cell throughput (increased cavity finesse). The ring-up time is related to the frequency sweep rate

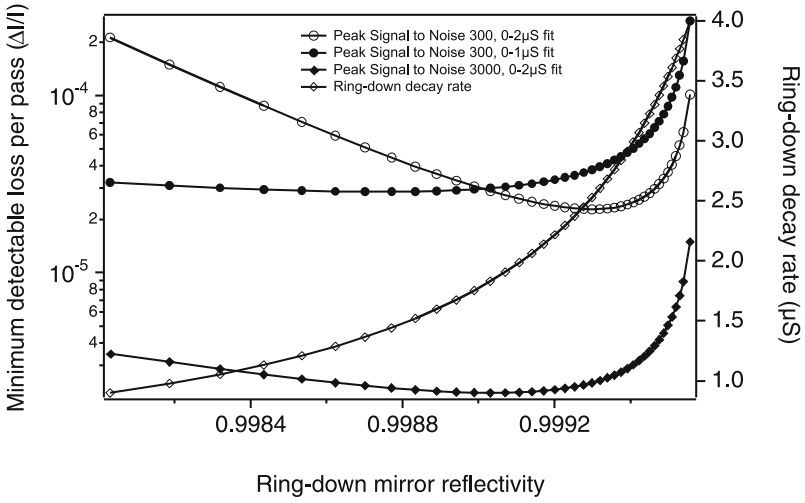

FIGURE 10 Predicted minimum detectable absorption based on semi-empirical noise model. Model inputs were based on peak observed signal at lowest measured reflectivity, noise for 100 averages, and fitting ranges from 0–1 and 0–2 μS. Extrapolated performance is given for 10× current peak signal

more intuitive minimum detectable absorption per pass. We assume here that the noise sources are constant with DFG power. The model does not incorporate wavelength dependent noise such as etalon effects or the effects of different ring-down cell modes and so is not completely quantitative. However, it does serve to illuminate key performance features.

Figure 10 illustrates the predicted minimum detectable absorption limit of the current system (expressed in minimum detectable loss per pass) and that of a similar system but with 10× greater power. For the current system, the operating wavelength range was restricted on one end by the ring-down cell throughput and on the other end by the low rf bandwidth of the detector amplifier combination (~ 2 MHz). Clearly, a higher power system is desirable. We observe experimentally that for a ring-down mirror reflectivity of 0.9992, the minimum detectable loss per pass is approximately 2×10^{-5}, which agrees well with the model. This was observed to increase to 5×10^{-5}, at a reflectivity of 0.9982 which is a factor of two larger than the predicted value. Taking a typical range of absorption cross sections for large organic molecules of 1×10^{-20} cm^2 to 1×10^{-18} cm^2 and a minimum detectable absorption of 2×10^{-5} per pass, this corresponds to a detection sensitivity of 5–500 ppb.

For a 10× increase in power (20–40 μW), the minimum detectable absorption per pass should be on the order 2×10^{-6} or 3.7×10^{-8} cm^{-1} for a 53 cm cell length. Higher power operation may be achieved through quasi-cw operation of the fiber amplifiers or through the use of coiled, large mode area fiber amplifiers, although these are currently available only for ytterbium or erbium -doped fibers. Based on the current system, we could expect a factor of two or more increase in performance for the praseodymium amplifier and with quasi-cw operation of the erbium amplifier or a large mode area fiber, a factor of five or more increase in power could be expected. These factors, combined with anti-reflection coatings on the crystal facets could yield a factor of 20 or more increase in DFG power. We have observed that if the seed to the erbium doped fiber amplifier is shut off briefly (~ 20 μS) and then switched back on, the peak power can easily be increased by a factor of 10 or more, although care must be taken to avoid damage and the onset of nonlinear phenomenon in the fiber. Quasi-cw operation with a low duty cycle could be problematic for overlapping of the DFG frequency with a ring-down cavity mode. Careful mode matching is equally important to ensure the highest throughput and reduction of wavelength dependent effects. For tuning related noise, a cavity locked approach could be used but this may require a ring cavity such as employed by Paldus et al. [28, 29]. This ensures that only a single mode is averaged and enables higher repetition rates although this adds complexity. Integrated cavity output spectroscopy (ICOS) offers an alternative to cavity ring-down spectroscopy but has a high spectral density of modes thus nearly eliminating the issue of mode overlap. Al-

though sensitivity can be high, normalization of the output signal is required which could introduce systematic noise.

A key challenge of this system will be to detect broadly absorbing, low-vapor pressure high molecular weight compounds. At typical atmospheric conditions, these may be too difficult to detect and may require preconcentration. Purge-trap methods of preconcentration are well established for increasing gas concentration in gas-chromatography, mass spectrometry systems and have recently been applied to cavity ring-down spectroscopy [26, 27]. Depending on the volume of air sampled, enhancement factors can easily be 100 or more. Combined with an optimized minimum detectable absorption of 10^{-6} /pass and peak absorption cross section of $1 \times 10^{-19}\,\mathrm{cm}^2$, detection sensitivities could approach the 10 ppt level. In reality, S/N ratios of 10 or more are usually desired so practical sensitivities would be on the order of a few hundred ppt for an optimized system with preconcentration. Other improvements such as real-time optimization of fitting parameters could improve performance but this is not expected to be a major improvement. For example, for shorter decays, higher sampling rates and shorter fit ranges are desired whereas for longer decays lower sampling rates and longer fit ranges are desired (Fig. 9).

4 Conclusion

Difference frequency mixing of telecom sources in OP-GaAs has been shown to be an effective method for the generation of broadly tunable, spectroscopic grade light in the long-wave infrared. With a single period OP-GaAs crystal, combined with both temperature tuning and pump tuning, over $300\,\mathrm{cm}^{-1}$ (100 nm) of tuning has been demonstrated. With multi-period crystals, this range could be extended to cover the entire difference of the "O" and "C" telecom bands. Alternatively, use of "O" and "S" band telecom sources could enable tuning throughout the 8–12 μm atmospheric window. The use of mature telecom band sources offers the attractive feature of transferring the tuning to the pump sources where technology is mature.

Although for this work the output power was low, this could be improved through the use of coated OP-GaAs crystal facets (approximately 40% improvement if coated for all wavelengths). Higher pump power could also be used, although care must be taken to avoid excessive linear absorption and 2-photon absorption, as the pump wavelengths are more than one-half of the bandgap of GaAs. We estimate that with quasi-cw operation of the fiber amplifiers, the output of the erbium fiber amplifier could be increased to the 10–20 W level and the output of the praseodymium amplifier increased to the 100 mW level. This, combined with AR coatings could easily increase the DFG output power a factor of 20 or more.

OP-GaAs also possesses another important attribute: namely cubic crystal symmetry, which can relax polarization constraints of the pump laser, allowing in some cases, the use of unpolarized light such as from an unpolarized fiber amplifier. However, the output DFG polarization would also be unpolarized. OP-GaAs should prove especially powerful for detection of broadly absorbing species. When combined with ultra-sensitive absorption methods such as cavity ring-down spectroscopy, OP-GaAs could be a valuable material for use in detection of large molecular weight, low vapor pressure molecules.

ACKNOWLEDGEMENTS We gratefully acknowledge the support of Ricky Sommers for the fabrication of custom electronic amplifiers and dynamic triggering circuits used in this work. We also thank Karla Armstrong for her assistance in the fabrication of the praseodymium-doped fiber amplifier. This research was supported by the US Department of Energy, Office of Nonproliferation and National Security, Office of Research and Development.

REFERENCES

1 I.T. Sorokina, K.L. Vodopyanov, *Solid State Mid-Infrared Laser Sources*, (Springer-Verlag, Topics in Applied Physics, Berlin, Heidelberg, New York, 2003)
2 T.J. Kulp, S.E. Bisson, R.P. Bambha, T.A. Reichardt, U.B. Goers, K.W. Aniolek, D.A.V. Kliner, B.A. Richman, K.M. Armstrong, R. Sommers, R. Schmitt, P.E. Powers, O. Levi, T. Pinguet, M.M. Fejer, J.P. Kplow, L. Goldberg, T.G. Mcrae, Appl. Phys. B **75**, 317 (2002)
3 M. Sieter, M. Sigrist, Infrared Phys. Technol. **41**, 259 (2000)
4 K.P. Petrov, R.F. Curl, F.K. Tittel, Appl. Phys. B **66**, 531 (1998)
5 S.E. Bisson, K.M. Armstrong, T.J. Kulp, M. Hartings, Appl. Opt. **40**, 4904 (2001)
6 B.A. Richman, K.W. Aniolek, T.J. Kulp, S.E. Bisson, J. Opt. Soc. Am. **17**, 1233 (2000)
7 K.W. Aniolek, T.J. Kulp, B.A. Richman, S.E. Bisson, Chem. Phys. Lett. **302**, 555 (1999)
8 L.A. Eyres, P.J. Tourreau, T.J. Pinguet, C.B. Ebert, J.S. Harris, M.M. Fejer, L. Becouarn, B. Gerard, E. Lallier, Appl. Phys. Lett. **79**, 904 (2001)
9 C. Gmachl, F. Capsso, D.L. Sivco, A.Y. Cho, Rep. Prog. Phys. **64**, 1533 (2001)
10 G. Wysocki, R.F. Curl, F.K. Tittel, R. Maulini, J.M. Bulliard, J. Faist, Appl. Phys. B **81**, 769 (2005)
11 D. Richter, D.G. Lancaster, R.F. Curl, W. Neu, F.K. Tittel, Appl. Phys. B **67**, 347 (1998)
12 D. Richter, D.G. Lancaster, F.K. Tittel, Appl. Opt. **39**, 4444 (2000)
13 F.K. Tittel, D. Richter, A. Fried, in *Solid-State Mid-Infrared Laser Sources*, ed. by I.T. Sorokina, K.L. Vodopyanov (Springer-Verlag, Topics in Applied Physics, Berlin, Heidelberg, New York, 2003)
14 W. Chen, D. Boucher, F.K. Tittel, Recent Res. Dev. Appl. Phys. **5**, 27 (2002)
15 O. Levi, T.J. Pinguet, T. Skauli, L.A. Eyres, K.R. Parameswaran, J.S. Harris Jr., M.M. Fejer, T.J. Kulp, S.E. Bisson, B. Gerard, E. Lallier, L. Becouarn, Opt. Lett. **27**, 2091 (2002)
16 O. Levi, T. Pinguet, T. Skauli, L.A. Eyres, L. Scaccbarozzi, M.M. Fejer, J.S. Harris, T.J. Kulp, S. Bisson, B. Gerard, L. Becouarn, E. Lallier, in *OSA Trends in Optics and Photonics (TOPS)*, Conference on Lasers and Electro Optics (CLEO) (Optical Society of America, Washington DC, 2001), Vol. 56
17 Y. Nishida, M. Yamada, T. Kanamori, K. Kobayashi, J. Temmyo, S. Sudo, Y. Ohishi, IEEE J. Quantum Electron. **QE-34**, 1332 (1998)
18 P. Urquhart, IEEE J. Quantum Electron. **QE-28**, 1962 (1992)
19 D.G. Cooper, J.L. Dexter, R.D. Esman, IEEE J. Sel. Top. Quantum Electron. **1**, 14 (1995)
20 G.D. Boyd, D.A. Kleinman, J. Appl. Phys. **39**, 3597 (1968)
21 A.N. Pikthin, A.D. Yaskov, Sov. Phys. Semicond. **12**, 622 (1978)
22 K.J. Schulz, W.R. Simpson, Chem. Phys. Lett. **297**, 523 (1998)
23 SNLO code available at www.sandia.gov/imrl/XWEB1128/xxtal.htm
24 D.Z. Anderson, Appl. Opt. **23**, 2944 (1984)
25 N.M. Sampas, D. Anderson, Appl. Opt. **29**, 394 (1990)
26 B.A. Paldus, C.C. Harb, T.G. Spence, B. Wilke, J. Xie, J.S. Harris, R.N. Zare, J. Appl. Phys. **83** 3991 (1998)
27 B.A. Paldus, A.A. Kachanov, Can. J. Phys. **83**, 975 (2005)
28 A.M. Parks, R.E. Lindley, A.J. Orr-Ewing, Anal. Chem. **76**, 7329 (2004)
29 M.W. Todd, R.A. Provencal, T.G. Owano, B.A. Paldus, A. Kachanov, K.L. Vodopyanov, M. Hunter, S.L. Coy, J.I. Steinfeld, J.T. Arnold, Appl. Phys. B **75**, 367 (2002)